Journal of Spacecraft and Rockets

VOLUME 7 MARCH 1970 NUMBER 3

A Review of Contemporary Solid Rocket Motor Performance Prediction Techniques

W. H. Miller and D. K. Barrington
Rocketdyne, A Division of North American Rockwell Corporation, McGregor, Texas

Nomenclature

a = "linear" burning rate coefficient, $r = aP^n$
A = flow area, in.^{2} or ft^2
A_b = propellant burning surface area, in.^{2}
A_p = grain port cross-sectional flow area, in.^{2}
A_s = nozzle surface area, in.^{2}
c^* = delivered characteristic velocity. In instantaneous form, $c^* = g_c P_c A_t/\dot{w}_p$, fps
c_p = propellant specific heat, Btu/lbm-°R
C_D = mass flow factor, $C_D = g_c/c^*$, lbm/lbf-sec; or drag coefficient on particle
C_f = skin-frictional drag coefficient
C_F = delivered nozzle thrust coefficient, $C_F = F/P_c A_t$
C_W = discharge coefficient, Eq. (33)
D, D_t = grain and throat diameters, respectively, in.
D_p = particle diameter, μ
F = thrust, lbf
g_c = gravitational conversion, 32.17 lbm-ft/lbf-sec^2, where 1 lb force = 1 lb mass × $32.17/g_c$
G = $\dot{w}/A$, weight flow rate per unit of cross-sectional flow area, lbm/sec-in.^{2}
h = coefficient of heat transfer, Btu/hr-ft^2-°R
h_c = convective heat transfer coefficient, Btu/hr-ft^2-°R
H, h = total and static enthalpies, respectively, Btu/lbm
I_{sp} = propellant specific impulse, lbf-sec/lbm; I_{spd} = measured or deliverable value
J = mechanical equivalent of heat = 778.16 ft-lbf/Btu
k = thermal conductivity, Btu/hr-ft-°R
k_i = empirical constants and exponents ($i = 1, 2, \ldots$)
Kn = Knudsen number
K_n = burning surface-to-throat area ratio, A_b/A_t
L = grain length, in.; L/D = grain length/diameter
$\dot{m}$ = mass flow rate, $\dot{w}/g$, slug/sec
M = Mach number
$\mathfrak{M}$ = molecular weight, lbm/lbm-mole
n = linear burning rate pressure exponent
Nu = Nusselt number
P = pressure (static unless otherwise specified), lbf/in.^{2}
P_{bo} = chamber stagnation pressure at burnout, lbf/in.^{2}
Pr = Prandtl number
$\dot{q}$ = heat flux, Btu/hr-ft^2
Q = total heat loss, Btu
r = propellant "linear" burning rate, aP^n, in./sec

William Miller is a Member of the Technical Staff in the Internal Systems Group of the Engineering Design and Development Section at the Solid Rocket Division of Rocketdyne. He has been with Rocketdyne for six years and during this period has served as responsible engineer on research and development programs in the areas of solid rocket igniter design and internal ballistic, gas dynamic, and grain stress analysis, and as program manager for preparation of the NASA Design Criteria Monograph, "Solid Rocket Motor Performance Analysis and Prediction." Prior experience includes three years as an aerodynamicist with the Missile and Space Division of Douglas Aircraft and one year as a teaching-research assistant at the University of Texas and the Defense Research Laboratory in Austin, Texas. He holds B.S. and M.S. degrees in aerospace engineering (University of Texas 1960, 1966), has authored or co-authored seven published papers, and is a member of AIAA and Sigma Xi.

Donald Barrington also is a Member of the Technical Staff in the same group at Rocketdyne. He joined Rocketdyne in 1963. Since May 1965 he has been the principal engineering computer programer for the group and has written numerous ballistic performance prediction and heat-transfer analysis computer programs. His responsibilities include solid-propellant grain design and ballistic performance analysis. Since November 1968 he has been in charge of data reduction at the McGregor facility. He received his B.S. degree in mathematics from Baylor University in 1967. He is a member of the AIAA.

Presented as Paper 69-732 at the AIAA 5th Propulsion Joint Specialist Conference, U.S. Air Force Academy, Colo., June 9–13, 1969; submitted June 20, 1969; revision received January 7, 1970. Based on a survey conducted under Contract NAS3-11210 with the NASA Design Criteria Office, Lewis Research Center, during the preparation of a Design Criteria Monograph.[1]

r_b = propellant burning front progression rate, in./sec
R = radius, in.; or gas constant, $R_0/\mathfrak{M}$, lbf-ft/lbm-°R
R_h = hydraulic radius, $2A_p/$(port perimeter), in.
R_0 = universal gas constant = 1546 ft-lbf/lbm-mole-°R
R^* = radius of curvature at nozzle throat, in.
Re = Reynolds number
s = entropy, Btu/°R
t, t_b = time and burn time, respectively, sec
T = temperature, °R
T_{aw}, T_W = adiabatic wall temperature and wall temperature, respectively, °R
u = velocity, fps
V,V_c = volume and chamber free volume, respectively, in.^{3}
w = grain web thickness, in.
W = weight, lbm
$\dot{w}$ = weight flow rate = $\dot{m}g = \rho A u$, lbm/sec
α = erosive burning rate proportionality factor, $\alpha = 0.0288\ k_6\ c_p\mu^{0.2}\ Pr^{-0.667}$, Eq. (19); also initial nozzle divergence half-angle, deg, Eq. (35); also, Mach angle, deg, $\alpha = \sin^{-1}M^{-1}$, Eq. (34); also, Stefan-Boltzman constant, Eq. (39); also wall inclination angle, deg, Eq. (38)
β = erosive burning rate constant, $\beta = (G \ln h_0/h)/r_b\rho_p$ Eq. (19); also, nozzle entrance convergence half-angle, deg
γ = ratio of specific heats
δ = burning rate augmentation term, Eq. (13)
ϵ = nozzle exit to throat area ratio, A_e/A_t
$\dot{\epsilon}$ = instantaneous erosion rate, in./sec
ϵ_T = particle cloud emissivity, Eq. (39)
θ_{ex} = nozzle exit plane lip angle, deg
λ = divergence loss factor, Eqs. (35) and (36)
μ = gas viscosity, lbm/ft-sec
π_K, $\pi_{P/r}$ = temperature sensitivities of pressure at particular values of K_n and P/r, respectively; $\pi_K = (\partial \ln P/\partial T)_{K_n}$, and $\pi_{P/r} = (\partial \ln P/\partial T)_{P/r}$
ρ,ρ_p = gas density, lbm/ft^3, and propellant density, lbm/in.^{3}, respectively
σ_K, σ_P = temperature sensitivities of burning rate at particular values of K_n and P, respectively; $\sigma_K = (\partial \ln r/\partial T)_{K_n}$, and $\sigma_P = (\partial \ln r/\partial T)_P$
τ_R = residence time, sec
φ = angle between local velocity vector and motor center line, deg
ψ = stream thrust/flow area = $P + \rho u^2/g_c$, lbf/in.^{2}

Superscripts

$'$ = conical nozzle point source model parameters
0 = theoretical value

Subscripts

a = ambient
bem = ballistic evaluation motor
bl = boundary layer
c = local stagnation combustion chamber
e = nozzle exit plane
fsm = full-scale motor
g = gaseous combustion products
i = ideal; or initiation of shock-turbulent boundary-layer interaction
ig = igniter
inc = incompressible
mem = material evaluation motor
0 = condition of motor and propellant just before ignition
p = propellant (except A_p = port area and D_p = particle diameter)
ref = value at reference conditions
s = separation
t = nozzle throat
tv = threshold value
vac = vacuum

Introduction

THIS paper reviews state-of-the-art techniques for predicting performance of contemporary solid rocket motor designs. Analytical techniques used in these predictions mathematically model 1) the generation and flow of combustion products within the combustion chamber; 2) propellant ballistic characteristics; 3) the influence of combustion chamber conditioning and operational environments on these propellant parameters; and 4) nozzle performance parameters, throat area, and thrust coefficients. Effects of temperature, pressure, mass addition, "erosive" burning, and acceleration on motor ballistic performance are treated for both steady-state and transient conditions. This review encompasses specific impulse and nozzle performance predictions, as well as burning rate and specific impulse testing and scaling. Combustion instability is another important facet of rocket design and performance prediction, and all rocket programs should include an early assessment of the combustion instability question, using available prediction techniques such as reviewed in Refs. 2 and 3. However, further discussion of combustion instability is beyond the scope of this survey.

Internal Flowfield Modeling

Three distinct phases, ignition, quasi-steady state, and bleed-down (or "tail-off") are seen in typical thrust- and pressure-time histories of contemporary solid rocket motors. Prediction of combustion chamber gas flow and mass generation for each is based on one-dimensional gasdynamic and thermodynamic relationships with proper consideration for conservation of mass, momentum, and energy.[4-9]

Steady-state gasdynamic relationships are used to describe motor performance during that phase in which the rate of change of chamber pressure is too small to influence ballistic parameters. Interior ballistics under this condition (quasi-steady-state) are predicted by one of two methods. Both assume a one-dimensional, adiabatic flow that complies to the perfect gas law and exhibits negligible friction losses. The first is applicable if pressure is essentially constant throughout the combustion chamber. It is used with end-burning grain configurations and with radial burners of low volumetric loading in which the Mach number in the grain port is low enough that pressure drop along the length of the grain is negligible. Under these conditions (Ref. 8, p. 239)

$$P_c = (A_b a \rho_p c^*/A_t g_c)^{1/(1-n)} \tag{1}$$

The second method is required with the occurrence of significant pressure drop along the axis of flow typical of a higher-performance motor with low port-to-throat area ratio. A one-dimensional, steady-state model is assumed, and the gas flow is evaluated incrementally as depicted in Fig. 1.

Applying the momentum equation to this element and assuming steady flow,[10]

$$P_2 = P_1 - 2(\dot{m}_2 u_2 - \dot{m}_1 u_1)/(A_1 + A_2) \tag{2}$$

A series of these increments is assumed down the length of the grain. Variations in flow area, burning surface area, and burning rate may occur between increments. The usual procedure is to approximate a head-end pressure by Eq. (1) and thus establish the gas generation conditions at that point. (Combustion product addition is at zero longitudinal velocity, Fig. 1.) Mass flow rate, port flow area, and approximated pressure are then used to predict the gas velocity and the mass being generated in the second increment, etc., until a nozzle-entrance pressure is obtained. Predicted nozzle entrance stagnation pressure calculated from the energy equation assuming isentropic flow

$$P_c = P[1 + (u^2/\gamma g_c RT)(\gamma - 1)/2]^{\gamma/(\gamma-1)} \tag{3}$$

is compared with that calculated from the continuity equation

$$P_c = \dot{m}_t \frac{c^*}{A_t} = \left[\rho_p \sum_{i=1}^{i=n} \frac{(\Delta V_p)_i}{\Delta t}\right] \frac{c^*}{A_t g_c} \tag{4}$$

This incremental evaluation and summation is repeated until these two values agree typically to within ±0.5%. Thrust is calculated by combining the resulting P_c and mass flow rate with the proper propellant and nozzle parameters

$$F = P_c A_t C_F = \dot{w}_p I_{spd} \quad (5)$$

This procedure is repeated for each interval of burn time for which motor thrust, pressure, and mass flow rate values are predicted.

Transient Performance

The rate of combustion product generation must equal the nozzle mass discharge rate plus the mass rate of accumulation in the chamber;

$$\rho_p A_b r_b = \dot{w}_t + d(\rho_c V_c)/dt \quad (6)$$

In applying this equation, it is frequently assumed that changes in V_c, combustion temperature T_c, and characteristic velocity c^* are negligible. Then Eq. (6) can be expressed as[8]

$$dP_c/dt = (\rho_p A_b r_b - A_t P_c C_D) R T_c / V_c \quad (7)$$

For incremental analyses, Eq. (2) is modified for transient flow to account for mass stored within each control volume. Then

$$\dot{w}_t = \sum_{i=1}^{i=n} \left[\rho_p A_{b_i} r_{b_i} - \frac{d(\rho_g V_c)_i}{dt} \right] \quad (8)$$

The variation of V_c due to propellant consumption is significant in certain applications. A successful technique has been to express V_c as a function of initial volume V_{c_0}, burning surface A_b, and grain web thickness w[11]:

$$V_c = V_{c_0} + \int A_b dw \quad (9)$$

Substitution of (9) in (6) yields

$$dP_c/dw = (\rho_p A_b - A_t C_D P_c^{1-n}/a)(RT_c/V_c) - A_b P_c/V_c \quad (10)$$

Ignition transient predictions must consider weight flow from the igniter ($\dot{w}_{ig}$), and the rate of flame propagation over the propellant grain burning surface [$A_b = A_b(t)$], so that Eq. (7) becomes[6]

$$dP_c/dt = [\dot{w}_{ig} + r_b \rho_p A_b(t) - P_c A_t C_D] R T_c / V_c \quad (11)$$

It is assumed that 1) T_c and P_c are uniform throughout the motor, 2) perfect gas laws are valid, 3) igniter gas has the same temperature and heat capacity as propellant gas, 4) $A_b(t)$ is a function of flame propagation rate,[12] and 5) the nozzle throat is choked ($M_t = 1$).

The $\dot{w}_{ig}$ predicted from ballistic analysis is generally confirmed by igniter demonstration firings,[12] and $r_b \rho_p A_b(t)$ is calculated from an incremental element analysis; $A_b(t)$ is influenced by the dependency of r_b on chamber pressurization, mass flux, grain temperature, and vehicle acceleration as well as ignition flame spreading rate. Although ignition theories exist, prediction of flame spreading is characteristically based on empirical data from past correlations.

Bleed-down accompanies the significant reduction in A_b typically encountered with propellant burnout or boost-sustain type transitions. Equation (7) is used, and the possible influence of depressurization on r_b is acknowledged. After propellant burnout, the first term of Eq. (7) drops out,

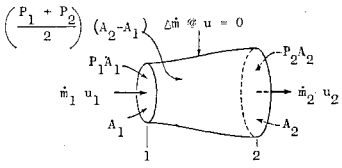

Fig. 1 Incremental flow control volume.

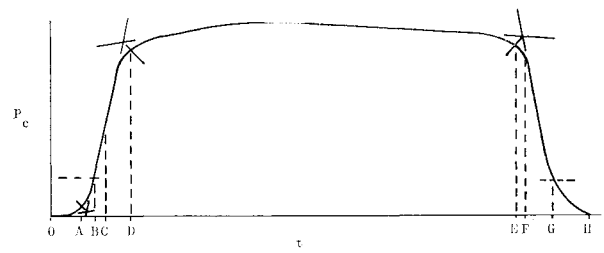

Fig. 2 Burn-time definition.

and the resulting expression can be solved for P_c as a function of bleed-down time:

$$P_c = P_{bo} \exp(-RT_c A_t C_D t / V_c) \quad (12)$$

Burning Front Progression

Propellant burning rate r_b depends on propellant composition and conditioning, combustion chamber environment, and vehicle dynamics. Since P_c usually has a strong effect on r_b, empirical expressions of the form

$$r_b = aP^n(1 + \delta) \equiv r(1 + \delta) \quad (13)$$

are often used. Here $r \equiv aP_c^n$ is called the "linear" burning rate, and the "augmentation" term δ accounts for an effect of vehicle spin, erosive burning, or some other phenomenon.

Linear Burning Rates

Current practice is to determine r over specified operational pressure and temperature ranges utilizing small ballistic evaluation motors (BEM's). The BEM's used throughout industry differ in size, grain configuration, and burning duration. They are typically 2 in. to 6 in. in diameter and provide near neutral pressure traces with sharp tail-offs. Grain web thicknesses are kept small to minimize the effects of thermal shrinkage. The port-to-throat area ratio A_p/A_t is generally greater than six to minimize the influence of erosive burning. Some BEM's are designed purposely to produce nonneutral pressure traces to permit evaluation of $r(P_c)$ in a single firing. Although this reduces the number of BEM's required, it does not provide as accurate a determination of the pressure exponent n.[1]

Burning rate is determined by dividing propellant web thickness w by burn time t_b. While w is readily measured, establishment of t_b involves the identification of surface ignition time and web burnout time on the pressure-time trace (Fig. 2). Several techniques are used,[13-15] and no one has proven superior in all applications. The surface ignition time has been identified with various points on the primary rise portion of the trace (Fig. 2): 1) the inverse tangent-bisector (point A), 2) a fixed pressure or a fixed percentage of the average or maximum pressure (point B),[15,16] 3) the initial inflection (point C), or 4) the tangent-bisector (point D). Web burnout time has been identified with 1) the aft tangent-bisector (point E),[13,15] 2) the point of maximum rate of change of curvature during tail-off (point F),[14,15] or 3) a fixed pressure or fixed percentage of the average or maximum pressure (point G).[15] One method[17] that may minimize motor-to-motor variations (due to sliver or nozzle erosion effects on the tail-off, for example) is to determine burn time by

$$t_b = (t_E - t_D) \int_0^H P_c dt \Big/ \int_D^E P_c dt \quad (14)$$

Ballistic motor rates frequently must be scaled 1% to 3% to correlate with full-scale motor (FSM) rates.[16,18,19] Where the diameters of the FSM's were an order of magnitude larger than those of the BEM's, 5% to 7% scale-up has been required. Largest values were required for FSM's with

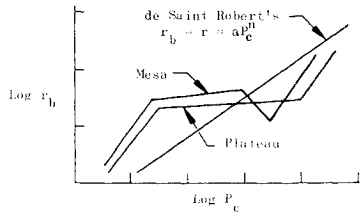

Fig. 3 Propellant burning rate-pressure relationships.

fiberglass cases, where changes in w occur due to combined propellant and case expansion upon motor pressurization. Another strain-inducing factor is propellant thermal shrinkage. Both factors lead to a slight reduction in w and frequently to an increase in A_b. Failure to acknowledge these factors analytically accentuates the apparent scale-up. Reviews[13,16] of discrepancies between BEM and FSM rates have concluded, however, that the primary contributor to the disagreement is inconsistent definition of BEM burn time.

Figure 3 depicts various $r_b(P_c)$ characteristics. The straight line represents de Saint Robert's linear burning rate equation, $r = aP_c^n$. Propellants showing a region of markedly reduced pressure exponent n are known as "plateau" propellants. Certain double-base propellants containing small amounts of lead compounds and some polymer binder-ammonium perchlorate composites exhibit a reduced n.[8] Propellants that show negative values of n over short pressure ranges are known, from the shape of the curves, as "mesa" propellants.

The number of tests employed to establish $r_b(P_c)$ depends on prior experience with similar propellants, the apparent linearity (or lack of it) over the pressure range of interest, the desired probability and confidence levels, and program economics and scheduling. Review of industrial practice indicated that over a pressure range in which a and n remain constant, a minimum of seven motors are fired at motor nominal operating temperature (two each at the lowest and highest expected P_c's and three at the nominal P_c), and five are fired at the expected temperature extremes. A large operating pressure range, as encountered in boost-sustain applications could require additional tests, because certain basically linear burning rate type formulations have exhibited significant variations in n at extremely low and high pressures. Such variations appear to be more prominent for formulations with relatively low burning rates ($r_b <$ 0.6 in./sec at 1000 psia and 70°F).

BEM data are used to determine empirical coefficients (π_k, σ_p, σ_k, $\pi_{P/r}$) that describe the sensitivity of r_b and P_c to propellant conditioning temperature, T_0. The most frequently used coefficients, σ_p and π_k, are related by

$$\sigma_p = (1 - n)\pi_k \tag{15}$$

In motors where pressure drop in the chamber is not large the effect of T_0 on P_c is calculated by

$$P_c = P_{\text{ref}} \exp[\pi_k(T_0 - T_{\text{ref}})] \tag{16}$$

However, in analyses involving significant flow velocity in the grain port, motor performance is better evaluated by consideration of T_0 effects on the burning rate coefficient a by

$$a = a_{\text{ref}} \exp[\sigma_p(T_0 - T_{\text{ref}})] \tag{17}$$

Typical values range from 0.05 to 0.12%/°F for σ_p and 0.1 to 0.2%/°F for π_k for composite propellants. For nitrate propellant values of 0.1 to 0.2%/°F and 0.2 to 0.4%/°F, respectively, are typical.

With low A_p/A_t, erosive burning becomes important, especially in the prediction of the high pressure peak accompanying ignition. Nonuniform surface regression that results down the length of the grain also influences tail-off characteristics. It has been noted[20-25] that 1) slow-burning propellants are more erosive than fast-burning propellants, 2) there is a threshold gas velocity and mass flux (Fig. 4) below which erosive burning does not occur, but it is not known whether the threshold value is a real or an apparent effect, 3) temperature of gas in the flow conduit appears to have no effect on erosive burning, and 4) propellant grain geometry influences erosive burning. Gas velocity, mass flux or Mach number values at which augmentation begins are frequently related to operating pressure semi-empirically. Such an expression for mass flux is

$$G_{tv} = k_1 + k_2 P_c^{k_3} + k_4 P_c^{k_5} \tag{18}$$

In treating erosive burning analytically one of the most successfully used semiempirical expressions was developed by Lenoir and Robillard.[27] Their model combines aspects of fluid flow and heat transfer and postulates a central core of flowing combustion gases surrounded by transpiring propellant walls. The augmentation term δ in Eq. (13) is related to heat flow acting through convection and thus dependent upon combustion-gas flow rate. The following burning rate expression results:

$$r_b = r[1 + \alpha G^{0.8} \exp(-\beta r_b \rho_p / G)/rL^{0.2}] \tag{19}$$

where β is a proportionality constant in relationship between the heat-transfer coefficient h under conditions of transpiration and the coefficient h_0 for zero transpiration, i.e., $h = h_0 \exp(-\beta r_b \rho_p / G)$, and where $\alpha \equiv (0.0288 k_6) c_p \mu^{0.2} Pr^{-0.667}$ and results from the postulation that $\delta = k_6 h/r$ and utilizes the Chilton-Colburn expression for turbulent flow over a flat plate, i.e., $h_0 = 0.0288 G c_p Re^{-0.2} P_2^{-0.667}$.

However, empirical expressions typified by those of Kreidler and Peretz or Saderholm have been used effectively. Kreidler's expression[26] (recently examined by Peretz[28]) is

$$r_b = r[1 + k_7(G - G_{tv})/P^{k_8}] \tag{20}$$

Saderholm[29] has related r_b to P_c and Mach number empirically by

$$r_b = \begin{cases} r(M/M_{tv})^{k_9}, & \text{for } M_{tv} < M \leq 0.5 \\ k_{10}(MP_c)^{k_{11}}, & \text{for } M > 0.5 \end{cases} \tag{21}$$

Recent data reported by Viles[30] (Fig. 5) indicate a relationship such as

$$r_b = r(P_c/k_{12})^{F(M)} \text{ for } P_c \geq k_{12} \tag{22}$$

Motor designs used in erosive burning tests are 1) high L/D motors with low A_p/A_t in which static pressures fore and aft of the grain are measured[26,28,31] and 2) propellant

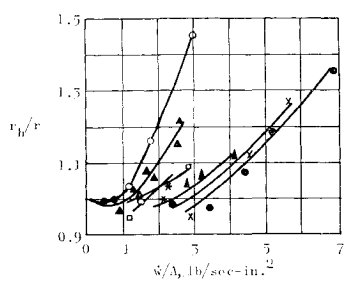

Fig. 4. Typical effect of mass flux on burning rate augmentation.[26]

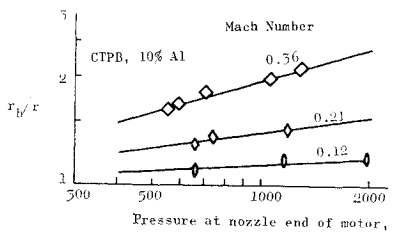

Fig. 5 Typical effect of Mach number and pressure on burning rate augmentation.[30]

slabs, flat or cylindrical, downstream of a larger gas generator.[25,27,30] The generator and slab propellant are the same; pressures are measured fore and aft of the slab; and pressures, mass flow, and Mach number are varied by geometrical changes in A_t, generator burning surface, and flow area past the slab. Erosive burning rate augmentation demonstrated in these tests is frequently scaled to predict full-scale motor augmentation using a ratio of the hydraulic radii,

$$\delta_{fsm} = \delta_{bem}(R_{hbem}/R_{hfsm})^{0.2} \quad (23)$$

The hydraulic radius has also been used quite successfully by some in place of grain length L in Eq. (19). This substitution has provided better correlations for narrow-slotted grain designs.

Pressure Augmentation

Von Elbe[32] originally developed the burning rate pressure transient relationship

$$r_b = r[1 + (k_{13}nk_p/c_p\rho_p r^2 P_c)(dP_c/dt)] \quad (24)$$

For the value of k_{13}, Von Elbe uses 2.0. With chamber pressurization, the effective regression rate is higher than the steady-state burning rate for the corresponding instantaneous pressure. Likewise, with chamber depressurization, the regression rate becomes less than that for steady-state conditions. Other investigators such as Paul et al.[33] and Parker and Summerfield[34] have developed similar relationships. These differ basically only in the value of the proportionality constant k_{13}; Paul et al.[33] use 1.0, and Parker and Summerfield[34] use 0.5.

Spin Augmentation

Burning rate augmentation produced by the spinning of a rocket motor about its longitudinal axis has been the subject of numerous studies. These studies, excellently reviewed in Refs. 35 and 36, reveal that augmentation is influenced by acceleration level, orientation of burning surface to acceleration vector, and metal content and particle size (Fig. 6). Empirically burning rate for the condition of spin has been expressed as[37]

$$r_b = r[1 + F(g)F(\theta)] \quad (25)$$

where $F(g)$ and $F(\theta)$ are functions of acceleration and surface orientation, respectively. Because of these dependencies, BEM's should be scaled replicas of FSM's. However, very valuable data can be obtained if propellant slabs are used as discussed by Northam.[38] Whitesides and Hodge[39] have recently prepared an internal ballistic computer program to treat effects of spin in pressure- and thrust-time predictions.

A recent compilation of rocket motor spin data,[35] indicates that centrifugal accelerations as low as 10 g directed perpendicularly into the burning surface of metallized solid propellants will: 1) increase ignition delay, 2) increase P_c and decrease t_b, 3) extend the tail-off burning period, 4) increase motor burnout mass through deposition of aluminum (oxide) on the chamber/nozzle walls, and 5) increase thermal protection requirements for the motor closures through increased convective heat transfer. Increased P_c and decreased t_b may be attributed to spin-induced burning-rate increases in radial burners. In end burners, surface area increases have been identified with propellant coning. The coning in turn has been related to a possible increased burning rate due to increased strain at the grain center (discussed in following section) and/or to the occurrence of a centerline vortex for motors with conventional converging-diverging nozzles.

Although certain analytical techniques have been developed,[36] their use in internal ballistic predictions is not currently considered state-of-the-art. This survey[36] led to

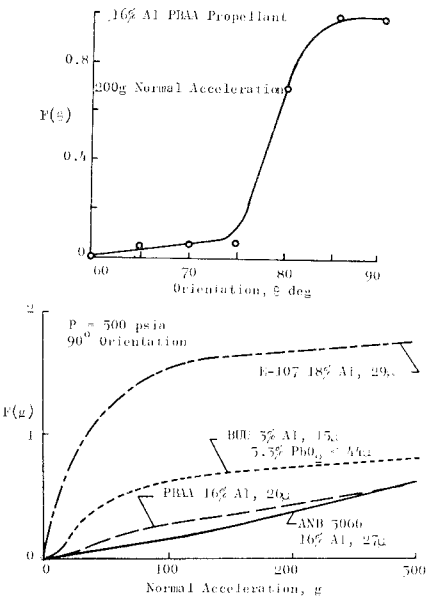

Fig. 6 Typical effects of orientation, normal acceleration, propellant formulations and Al particle size on burning rate.[37]

the following conclusions with regard to combustion chamber environment: 1) rotation reduces the discharge coefficient; 2) recirculating, viscous flow patterns can be established, and the boundary layer transports significant portions of the mass from one area of the flowfield to another; and 3) rotating flow establishes pressure gradients that may alter the local burning rates and can affect the combustion zone by retention of solid phases on the burning surface.

Strain Augmentation

For certain propellants, tests have indicated a strain-induced increase in r_b related to the compressibility of the propellant.[1,40,41] The more compressible the propellant (i.e., the greater the reduction in Poisson's ratio from the incompressible value of 0.5), the more significant was the increase in r_b. It should be noted, however, that a few tests revealed an opposite trend.[41]

Delivered Specific Impulse

Delivered specific impulse (I_{spd}) dependency not only includes 1) nozzle performance, 2) ambient condition, and 3) available combustion energy of the propellant, but also 4) energy lost from combustion gases to motor hardware, 5) extent of velocity and thermal equilibrium attained by gaseous and solid exhaust products, 6) combustion efficiency, i.e., the relative completeness of combustion in the motor chamber, and 7) contribution of discharged inerts. Maximum theoretical specific impulse, $I_{sp,}^0$ is predicted utilizing Gibbs minimization of free energy and assuming a one-dimensional, perfect thrust chamber, shifting equilibrium, and a totally gaseous medium. References 42 and 43 provide brief, comprehensive reviews of computer programs used by industry for these predictions.

Figure 7 is a typical example of the relative influence of the factors that contribute to the difference between I_{sp}^0 and I_{spd}. Techniques to evaluate most of the loss factors are available. However, only limited studies have been made for prediction of losses associated with combustion inefficiency and finite-rate chemical kinetics in a two-phase, axisymmetrical or two-dimensional flow. Particle-lag losses reflect mostly in characteristic velocity c^* rather than the thrust coefficient C_F. In fact, for large fractions of particles, Hoglund[44] has shown C_F increasing with the magnitude of lag for certain ranges of particle size. Thus, c^* cannot be

used as a measure of combustion efficiency for particle-laden combustion products. Most of the lag develops just upstream of the nozzle throat (sonic point) where the limiting mass flow is determined.[45]

Analytically predicted propellant performance is currently substantiated by BEM tests. These motors simulate, as closely as practical, conditions under which the full-scale

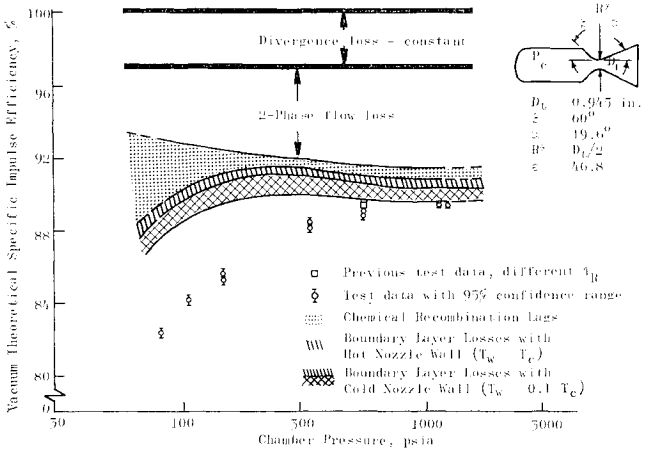

Fig. 7 Typical effect of chamber pressure on vacuum specific impulse efficiency (Ref. 1, adapted from Ref. 46).

motor will operate. This demonstrated performance is in turn scaled to deliverable FSM performance values by use of experimentally established data such as that shown in Fig. 8 or by analytical assessment of each loss factor as in Refs. 46 and 47.

Analytical Prediction

A limited number of computer programs presently combine thermal energy conversion and certain detailed flow calculations. Two such programs have been prepared by Kliegel et al., for the analytical prediction of specific impulse of two-phase media. The first is a one-dimensional, two-phase, reacting-gas, nonequilibrium performance program,[49] and the second treats an axisymmetric two-phase flow assuming a perfect gas[50] (i.e., gas phase expansion is treated as having a constant molecular weight and specific heat ratio). The one-dimensional program is completely self-contained, requiring specification only of the propellant system (elemental composition and heat of formation), relaxation rates, and nozzle geometry. The composition and heats of formulation data can be obtained from JANAF (Joint Army, Navy, Air Force) standard tables,[51] and some relaxation rate data have been published.[52] The program allows simultaneous consideration of both chemical and gas-particle relaxation losses in propellant systems having condensed exhaust products. It is written in FORTRAN IV and allows equilibrium, frozen, and kinetic performance calculations to be performed during a single machine run.

Except for Kliegel's one-dimensional nonequilibrium program, the analytical prediction of I_{spd} of a two-phase medium is made by degrading I_{sp}^0 calculated assuming infinite-rate,

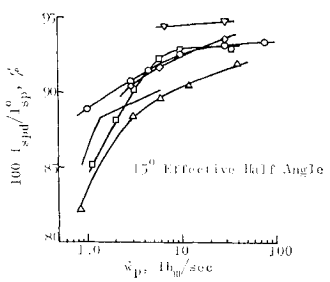

Fig. 8 Typical effect of mass flow rate on test motor I_{spd} efficiency for various propellants and geometries.[48]

shifting equilibrium. The programs developed at the NASA Lewis Research Center by Zeleznik and Gordon[53,54] are typical of the thermochemistry programs used in I_{sp}^0 calculations. In general, thermochemistry programs calculate

$$I_{sp}^0 = u_e/g_c + A_e(P_e - P_a)/\dot{w}_p \tag{26}$$

where

$$u_e = [2J(H_c - h_e)/g_c]^{1/2} \tag{27}$$

and

$$\dot{w}_p = \rho_e A_e u_e \tag{28}$$

where ρ_e is obtained from the equation of state. As reviewed briefly in Ref. 48, the determination of the chamber enthalpy H_c requires an iteration procedure where T_c is varied until H_c is equal to the potential enthalpy of the propellant H_p. Each time a new T_c is selected during the iteration, the chemical composition is determined so that the total free energy of Gibbs function of the gas mixture is minimized. The theory of minimizing the free energy includes both gas and condensed species. Chamber pressure is held constant during the iteration process. After T_c has been determined, the entropy s_c of the mixture is calculated. To find the exit static enthalpy h_e, the exit pressure P_e is set, and isentropic expansion along the nozzle from the chamber to the exit plane is assumed; then T_e is varied until $s_e = s_c$. Again, each time a new T_e is selected during the iteration, the chemical composition is determined by minimizing the total free energy.

If I_{spd} data are available, an empirical factor (I_{spd}/I_{sp}^0, Fig. 8) can be used to adjust I_{sp}^0. Alternatively, delivered C_F and c^* values and efficiencies are required. Delivered thrust coefficients are calculated using the gas dynamic analysis techniques, particle size, drag coefficients, etc. (i.e., as done by Crowe et al.[46] and Hoffman and Lorene[55]). This is discussed later under nozzle performance. Crowe et al.[46] found combustion efficiency to be very sensitive to residence time and pressure. Regarding P_c sensitivity (Fig. 7), the following trends were noted: 1) divergence loss is constant; 2) two-phase loss increases with pressure due to increased particle size; 3) based on Bray's sudden freezing criterion,[56] recombination loss decreases with pressure and approaches a constant magnitude, indicating reactions are nearly complete when the composition "freezes"; and 4) boundary layer and heat losses decrease slightly with increased P_c and throat radius according to

$$\Delta I_{sp}/I_{sp} \sim k_{14}(P_c R_t)^{-0.2} \tag{29}$$

Theory and experiment agreed well at high-pressure levels. At lower levels, however, demonstrated performance was considerably less than that predicted. Crowe concluded that residence time, defined as

$$\tau_R \equiv \rho_g V_c/\dot{w}_g \tag{30}$$

was the factor contributing to this additional loss. In these tests, V_c was increased to increase burning surface and operational pressure levels, which also resulted in an increased residence time. Small τ_R, corresponding to low P_c in Fig. 7,* implied incomplete combustion. This is corroborated further by earlier data also shown in Fig. 7. These data are for the same propellant and nozzle geometry and scale, but τ_R was 75% greater. Analytical models and techniques have not proven satisfactory for predicting combustion efficiency for all types of propellant, although a correlation in combustion efficiency between strands and small motors has been reported.[57] Combustion efficiency, therefore, remains an experimentally determined factor.

* With $n < 1$, w_g decreases by a smaller percentage than P_c and ρ_g, so that τ_R decreases as P_c decreases.

Demonstration

In some instances, BEM's are scaled replicas of the FSM, especially in the design of extremely large solid propulsion systems.[58] However, BEM's are more frequently of a simple design. Characteristically, they are radial burners, similar to those described in Ref. 48 and 59, and comply to the recommendation of the ICRPG Static Test Working Group.[48] The design should provide a neutral pressure-time trace (within $\pm 10\%$); a sharp tailoff, burn time $\geq 87\%$ of action time, and tail-off pressure integral $< 5\%$ of action time pressure integral†; and $A_p/A_t > 6$ and $L/D \leq 2$ to minimize erosive burning influence. Burning duration should be short (2–10 sec) to minimize heat loss and nozzle erosion. Nozzle throat insert material and size should be selected to minimize throat erosion and produce a P_c within $\pm 10\%$ of the FSM operational value. Nozzle geometry is typically conical, with a divergence half-angle of $15° \pm 0.5°$ and an expansion ratio slightly less than optimum to guarantee full-flow attachment throughout motor equilibrium burning. To permit an accurate measurement of propellant specific impulse, unwanted mass flow contributions due to inerts are avoided by the use of little or no liner. Consumed weight should be confirmed by prefiring and postfiring motor weight measurements. A propellant weight of about 50 lb is desirable to permit satisfactory scaling to large motors. For smaller FSM's ($D \leq 30$ in.) satisfactory scale-ups have been made from BEM's with 5-lb to 10-lb propellant charges. Examples of ballistic evaluation motors that meet these general requirements are the AFRPL (Air Force Rocket Propulsion Laboratory) BATES motor[59] and the Rohm and Haas 6C5-11.4 motor.[13]

Rohm and Haas,[13] Crowe et al.,[46] and Peterson[60] have conducted rather extensive tests to determine the primary considerations necessary in scaling I_{spd}. These studies concluded that calculated two-phase flow losses, when combined with nozzle divergence losses and experimentally determined heat losses for the BEM's, correctly account for most of the difference between I_{sp}^0 and I_{spd}. These factors plus recombination, submergence, frictional, etc., loss factors, and the contribution of inerts are evaluated for the FSM to predict I_{spd}. Reference 61 contains charts by which one can quickly and reliably predict the magnitude of performance loss due to two-phase flow in the nozzle. Evaluation of these factors is discussed under nozzle performance. The magnitude of inert products discharged during motor firing is predicted by heat-transfer analyses. Empirical values are often used for the $I_{sp_{inert}}$ of this inert material; they range from 120 to 200 lbf-scc/lbm[62] and depend on the oxidation ratio, i.e., the oxygen available within the chamber to support combustion of inerts. One accepted practice for inert liners having the same binder as the propellant is to use one-half the value of the propellant's I_{sp}^0. Gordon[63] developed an expression to relate insulation loss due to pyrolysis or erosion to the increase in I_{spd}.

Nozzle Performance

Throat Area Variations and Surface Roughness

Data used in predicting A_t variations are typically based on detailed heat transfer analyses and supported by subscale and/or material evaluation motor (MEM) tests. As much as 2.5% loss in I_{spd} efficiency has been attributed to nozzle erosion by burnout of a 55-sec duration motor.[48] This effect includes reduction in expansion ratio ϵ and increased surface roughness.

† Refer to Fig. 2; action time $= t_H - t_0$; t_b may be defined by Eq. (14). These stated constraints are desirable but may be relaxed, particularly with respect to tail-off, in early stages of development with new propellants.

Nozzle evaluation tests are conducted to verify or provide inputs to detailed heat-transfer analyses[58,64] as reviewed by Wong.[65] In such tests exhaust gas species P_c and $\dot{w}/A$ duplicate those expected in the full-scale motor. Lack of exact duplication of the latter two parameters can be approximated by scaling erosion rates utilizing Bartz's[66] simplified equation

$$\dot{\epsilon} = \dot{\epsilon}_{mem}(P_c/P_{c_{mem}})^{0.8}(D_{t_{mem}}/D_t)^{0.2} \tag{31}$$

Decreases in A_t are encountered when 1) nozzle inserts fabricated from noneroding material such as tungsten expand under continuous heating or 2) metal oxide is deposited on the nozzle throat surface during motor firing. Deposits are discharged when either the nozzle surface temperature attains the melting temperature of the metal oxide or the gasdynamic drag forces exceed the strength of the deposition. This deposition problem usually is neglected in initial performance predictions of a motor design.

Thrust Coefficient

For one-dimensional, isentropic flow in an idealized converging-diverging nozzle, thrust coefficient is expressed as[7]

$$C_{Fi} = \left\{\frac{2\gamma^2}{\gamma-1}\left(\frac{2}{\gamma+1}\right)^{(\gamma+1)/(\gamma-1)} \times \left[1 - \left(\frac{P_e}{P_c}\right)^{(\gamma-1)/\gamma}\right]\right\}^{1/2} + \left(\frac{P_e - P_a}{P_c}\right)\epsilon \tag{32}$$

Maximum C_{Fi} corresponding to any fixed pressure ratio P_c/P_a is achieved when $P_e = P_a$; vacuum conditions correspond to $P_a = 0$.

Considerable demonstrated motor and nozzle efficiency data have been accumulated by industry for contemporary designs. Frequently this has made it feasible to simply adjust C_{Fi} by previously demonstrated efficiencies to rather accurately predict nozzle performance for new but similar design applications.

Detailed prediction of delivered C_F for contemporary solid rocket motors requires analysis of high-temperature subsonic, transonic, and supersonic flowfields in which a two-phase medium, chemically in nonequilibrium, is gaining momentum through expansion. Simultaneously, the flow is losing energy due to friction, heat transfer, and radial expansion. The differential equations required to express this flow are elliptical in the subsonic regime; mixed in the transonic regime, $0.8 < M < 1.2$; parabolic at the sonic condition; and hyperbolic in the supersonic regime. As a result C_F is often calculated in two parts. The first is dependent on the discharge coefficient,

$$C_W = \frac{\dot{m}(\text{across transonic control surface})}{\dot{m}\ (\text{for } 1 - D \text{ flow through } A_t \text{ at } M = 1)} \tag{33}$$

Mass flow rate at the throat is predicted by numerically integrating the flow across the transonic control surface. Then the transonic control surface flow characteristics are used as inputs to a method-of-characteristics analysis of the supersonic flowfield in the nozzle exhaust cone. Total nozzle thrust coefficient is computed by summing the thrust at the transonic control surface and the pressure forces along the nozzle wall or by combining the total mass flow rate and the calculated velocity field across the exit control surface.[67–69] For vacuum conditions, this latter approach gives[69]

$$C_{F\,vac} = 2\pi \int_0^{Re/Rt} \left\{\frac{P}{P_c} + \frac{\rho u^2 \sin\alpha \cos\varphi}{P_c g_c \sin(\varphi + \alpha)}\right\} \frac{R}{R_t} d\left(\frac{R}{R_t}\right) \tag{34}$$

For conical nozzles the effect of nonaxial exhaust velocity is frequently treated by correcting by a divergence loss factor λ.[70–72] With point-source flow assumed, λ is expressed as

$$\lambda = (1 + \cos\alpha)/2 \tag{35}$$

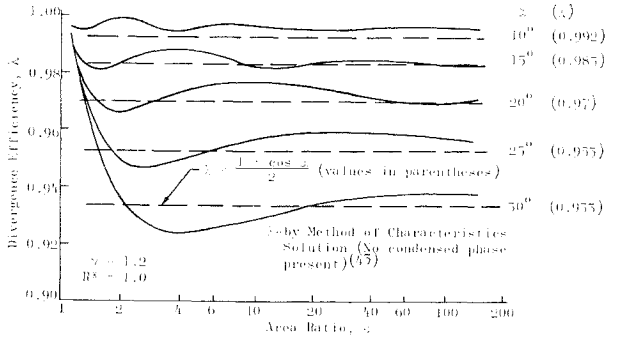

Fig. 9 Divergence efficiency for conical nozzles.

As pointed out by Rao[72]

$$C_{F_{\text{corrected}}} = \lambda C'_{F_i} \tag{36}$$

where C'_{F_i} is calculated as in Eq. (32) but the exit pressure P'_e and expansion ratio ϵ' are properly based on exit cone spherical area A'_e and critical area A'_t corresponding to the mass flow through the nozzle. Figure 9 compares the λ values predicted by Eq. (35) for conical nozzles with divergence loss factors predicted using two-dimensional, method of characteristics analyses as functions of ϵ for various α's. The latter set of data[43] includes both the effects of non-axially directed momentum at the nozzle exit and the throat curvature effect on the discharge coefficient.

Momentum losses incurred upstream of the nozzle throat significantly affect C_W. Qualitatively, entry contour and contraction ratio limitations account for 30% to 90% of these losses.[45,48,73] Viscous effects can account for 5% to 10% and submergence 25%. Submergence losses as reported by Kordig and Fuller[74] were relatively more significant. However, their study combined entrance loss factors. More recent data, Fig. 10, have isolated the influence of submergence, per se.[75]

Figure 11 illustrates a typical distribution of momentum losses as influenced by A_t (hence motor size; ϵ is fixed). Contemporary analyses were used by Crowe et al. to correlate with the motor data shown therein. Condensation and shock losses, estimated by some as 0.3 and 0.2%, respectively, can account in part for the correlation differences.

Two-Phase Flow

The effect of metal oxide particles in the exhaust products of solid rocket propulsion systems (Fig. 12) has been the subject of many reviews.[1,44,57] Losses result because of the velocity lag of the particles and their failure to transfer thermal energy to the gas. They gain motion only from drag forces exerted by combustion gas, and they transfer heat to the gas primarily by convection.

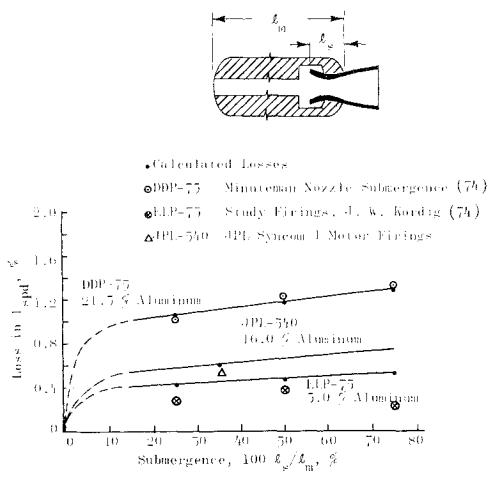

Fig. 10 Typical specific impulse losses from nozzle submergence.[75]

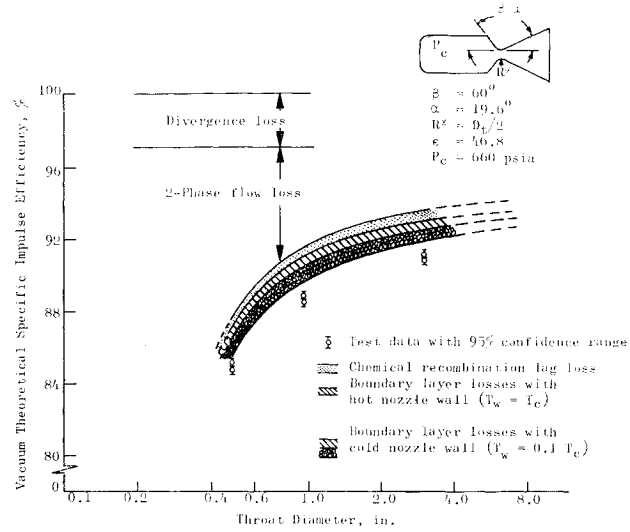

Fig. 11 Typical effect of throat diameter on vacuum specific impulse efficiency (Ref. 1, adapted from Ref. 46).

Programs have been prepared to analyze the flow of gas particles in one-dimensional,[13,49,61,76] and two-dimensional and axisymmetric nozzles.[50,77,78] As indicated in Ref. 42, other programs exist, but many have not been documented in the open literature. As with these documented referenced programs, their degrees of sophistication differ considerably. Finite-rate performance losses and nozzle boundary-layer and heat losses are not generally treated in these programs but are assessed separately.

Various analytical techniques are combined in solving the gas-particle flowfields. Two-dimensional potential flow theory[79] is applied in the solution of subsonic flowfields. However, the governing equations for gas-particle mixtures are elliptic in nature; thus, approximations assuming one-dimensional type flow or two-dimensional incompressible flow are often used. Analytical techniques used to predict two-phase flow in the transonic region are based on theory assuming a perfect gas but with the gas characteristics modified to account for the condensed phase.[50,77,78] For larger nozzle entrance radii, $R^*/R_t > 2$, and perfect gas flow, series solutions in terms of R^*, R_t, and γ have resulted from analyses of Oswatitsch,[80] Sauer,[81] and Hall.[82] An approximate method[83] for the transonic flow solution with smaller radii of curvature is an inverse solution of the transonic flowfield. For example, the calculated velocity distribution is adjusted until the boundary streamline corresponds to the desired real boundary. Steady irrotational, adiabatic, and shock-free flow of a perfect gas with constant specific heat is assumed in these analyses. As noted by Kliegel[45] all the characteristics of the governing flow equations are real if the flow is super-

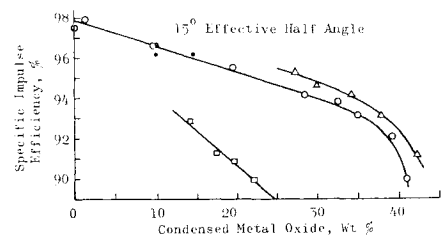

Fig. 12 Typical effect of condensed metal oxide in exhaust on test motor I_{spd} efficiency.[48]

Table 1 Drag coefficients for spherical particles

Semiempirical expressions	Ref.
$C_D = \frac{24}{Re}$, where $(R < 1.0)$	94, p. 97
$C_D = \frac{24}{Re}\left(1 + \frac{3\,Re}{16}\right)$, where $(R < 5)$	94, p. 98
$C_D = C_D^{(0)}\left[\frac{(1 + 7.5Kn)(1 + 2Kn) + 1.91Kn^2}{(1 + 7.5Kn)(1 + 3Kn) + (2.29 + 5.16Kn)Kn^2}\right]$	45
$C_D = \frac{24}{Re}\left[\frac{\{1 + 0.15Re^{0.687}\}\{1 + \exp[(0.427/M^{4.63}) - (3.0/Re^{0.88})]\}}{1 + (M)/(Re)[3.82 + 1.28\exp(-1.25\,Re/M)]}\right]$	88
$C_D = (C_{D\text{inc}} - 2)\exp\left[-3.07(\gamma)^{1/2}\frac{M}{Re}g(Re)\right] + \frac{h(M)}{\gamma^{1/2}M}\exp(-Re/2M) + 2$	
where $\log_{10} g(Re) = 1.25[1 + \tanh(0.77\log_{10}Re - 1.92)]$	93
and $h(M) = [2.3 + 1.7(T_p/T_g)^{1/2}] - 2.3\tanh(1.17\log_{10}M)$	

sonic. Thus, the solutions to the flow regime for a gas-particle mixture can be computed using the method of characteristics.[84,85]

Typical assumptions in these analyses are 1) the particles are spherical and of a specified size or sizes with a uniform internal temperature; 2) particles do not interact with each other and are of negligible volume; 3) total gas-particle mixture mass and energy are constant, and thermal energy is transferred by convection only; and 4) external forces, except gas pressure and particle drag, are negligible, and initial kinetic lags exist. Gas and particle specific heats are generally treated as being constant and have a value averaged for a two-phase medium.[47,49,50] It should be emphasized, however, that the accuracy of predicting nozzle performance with a two-phase medium is dependent not only on accurate solutions to the flow equations but also on the characteristics of the particles.

Particle characteristics that must be known or assumed to integrate the two-phase flow equations include particle shape, size, size distribution, and drag and heat transfer (Nusselt number) coefficients. The logarithmic normal size distributions used by Kliegel[45] remain consistent with the findings of many recent investigations.[1] Particle size measurements,[86–92] as made by direct sampling of the exhaust products and by optical in situ techniques, have been reported as functions of several variables, among which are chamber pressure, metal concentration, motor residence, thrust level, and motor size. Regarding the latter the expression

$$D_p = 3.25D_t^{(0.52 - 0.56\times10^{-2}Dt + 0.35\times10^{-4}Dt^2)} \quad (37)$$

for particle diameter (D_p, μ) as a function of throat diameter (D_t, in.) was derived for $D_t \leq 90$ from data supplied by Beckman.[86] This expression is based on a curve fit of data obtained from firings of motors ranging in size from several inches up to 260 in. in diameter and includes a variety of propellant formulations. In a recent review,[87] Crowe and Willoughby concluded that residence time is the principal independent variable. Cheung and Cohen[92] depicted particle volume mean diameter as a function of residence time but also indicate that chamber pressure must be considered (see Fig. 13).

Numerous mathematical models have been developed to describe particle growth but have not been incorporated in state-of-the-art two-phase nozzle performance programs. From experimental data, as summarized in Ref. 1, various semiempirical relationships have been suggested for the expression of particle drag coefficient, Table 1, and Nusselt number, Table 2. All investigations have been conducted under the assumption that the particles are spherical. The Reynolds number is based on the particle-gas lag velocity increment. Recent works by Crowe et al.[93] and Carlson and Hoglund[88] indicate that particles encounter the complete gamut of flow regimes from continuum to free-molecule flow. Semiempirical expressions for particle drag over these regimes are developed in the referenced reports[44,88,93–96] along with Kliegel's expression[45] which corrects for slip flow.

Table 2 Nusselt numbers for spherical particles

Semiempirical expressions	Ref.
$Nu = 2.3Re^{0.15} + 0.04Re$	
$Nu = 2 + 0.370Re^{0.6}Pr^{1/3}$	95
$Nu = 2 + 0.459Re^{0.55}Pr^{1/3}$	44
$Nu = \frac{Nu^{(0)}}{1 + 3.42(M)/(RePr)Nu^{(0)}}$	96
$Nu = \frac{2 + 0.459Re^{0.55}Pr^{0.33}}{1 + 3.42(M/RePr)(2 + 0.459Re^{0.55}Pr^{0.33})}$	88
$Nu = \frac{Nu^{(0)}}{1 + 2.72(Kn)/(\gamma^{1/2}Pr)Nu^{(0)}}$	45
$Nu = \left[(2 + 0.654Re^{1/2}Pr^{1/2})^{-1} + 3.42\frac{M}{RePr}\right]^{-1}$	

Recombination Losses

Idealized motor performance prediction thermochemistry programs typically assume chemical reactions to be either "frozen" or in "shifting" equilibrium with the gas flow process. In frozen flow predictions, the composition does not change during the expansion, but phase equilibrium is ob-

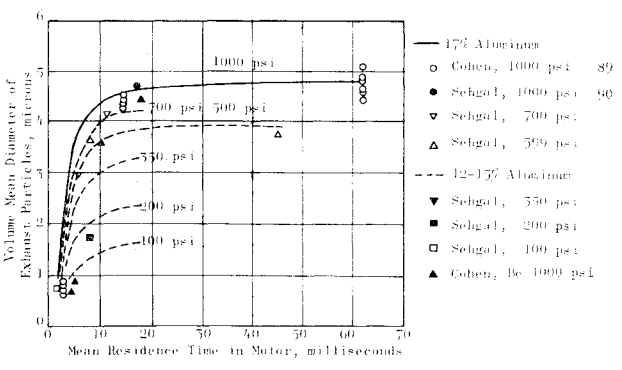

Fig. 13 Effect of residence time on exhaust particle size.[92]

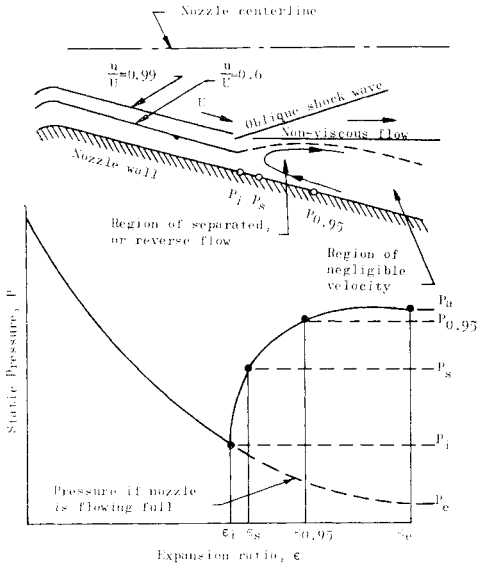

Fig. 14 Physical model of flow separation and static pressure characteristics.[100]

tained. In shifting equilibrium flow predictions, it is assumed that the chemical reaction rates are so fast that chemical equilibrium occurs continually as T and P drop during the expansion.[97] Equilibrium predictions provide an upper bound for theoretical performance. The programs prepared by Zeleznik and Gordon[53,54] are typical of those used in predicting frozen and equilibrium performance.

Real flow falls between the foregoing two extremes. Two basic types of finite-rate performance loss calculation techniques have been developed[42] to account for these losses. The first, an exact method, performs step-by-step integration of equations that describe an arbitrary set of relaxation or recombination of processes. The enthalpy and composition of the expanding nonequilibrium gas flow can be found at any point in the nozzle through the solution of these equations. An example of this type program is the one prepared by Kliegel et al.[49] for NASA Manned Space Flight Center.

The second method, an approximate solution, assumes that the nozzle flow can be divided into three successive regions: 1) equilibrium flow, 2) transition, and 3) frozen flow. Most approximate methods reduce the transition region to a point, called the sudden freezing point; this approach is typified by Bray's work.[56]

Boundary-Layer and Heat Losses

Analyses of two-phase flowfields and the determination of particle trajectories indicate that the boundary layer in solid-rocket nozzles will be composed primarily of gas with few particles.[98] An exception occurs only if the particles are so very small that they have no channeling tendency or if the nozzle is very long and the contour permits particle impact.[45] Therefore boundary-layer and heat-transfer analyses are typically made by assuming a gaseous medium without particles. The boundary layer is assumed to be turbulent and the solution is normally computed by employing a simultaneous solution of the integral momentum and energy equations as described by Elliott, Bartz, and Silver.[99] Examples of boundary-layer momentum and displacement thicknesses are given in Ref. 43. The influence of boundary-layer losses has often been neglected when it appears that viscous drag would not be significant because of the small surface areas on which viscous forces would act. To establish the true significance of the boundary-layer and heat losses, however, each loss must be evaluated with respect to the required accuracy of the performance prediction for the particular motor being analyzed.

If the subscript i is used to indicate ideal flow in a nozzle that is unaffected by a boundary layer, and choked conditions exist at the throat, the difference in thrust coefficient between an "ideal-flow" motor and a "real" motor can be expressed as

$$(\Delta C_F)_{bl} = \int_0^1 \frac{\psi_i - \psi}{P_c}\, d\left(\frac{A}{A_t}\right) + \int_{A_s/A_t} \left(\frac{P_i - P}{P_c}\sin\alpha + \frac{\rho u^2}{2P_c g_c} C_f \cos\alpha\right) d\left(\frac{A_s}{A_t}\right) \quad (38)$$

where ψ = stream thrust/flow area $= P + \rho u^2/g_c = P(1 + \gamma M^2)$, A_s is the local exit cone surface area, C_f is the skin-friction coefficient for the nozzle walls, and α is the local nozzle half-angle. The final term in (38) treats the effect of changes in nozzle wall pressure due to effective displacement of the flow boundaries and local heat transfer.

Convective heat flux distributions are predicted using heat-transfer coefficients as determined from the boundary-layer analysis and from the gasdynamics analysis of the local exhaust flowfield radiant heat flux[65]

$$\dot{q} = h_c(T_{aw} - T_w) + \epsilon_r \alpha (T_c^4 - T_w^4) \quad (39)$$

The $\dot{q}$ distribution is integrated over A_s for the action time of the motor. Thermal energy is then converted to an incremental specific impulse loss

$$\Delta I_{sp} = [2JQ(1 - T_e/T_c)/g_c W_p]^{1/2} \quad (40)$$

Flow Separation

When $P_e \lesssim P_a$, flow separation (Fig. 14) may occur. The result is an increase in nozzle surface pressure and a corresponding gain in thrust. Separation is often encountered in sea-level static tests of high-altitude (high-expansion ratio) nozzles. To account for the contribution to delivered performance, thrust coefficient is expressed as

$$C_{F\text{total}} = (C_F)_{\text{upstream of separation}} + (\Delta C_F)_{\text{downstream of separation}} - (P_a/P_c)\epsilon_e \quad (41)$$

Many empirical values have been used for the pressure and Mach number ratios at which flow separation occurs.[7,8,68,100-107] A general expression, determined by Kalt and Badal,[100] relates separation, ambient, and chamber pressures as

$$P_i/P_a = 0.667(P_a/P_c)^{0.2} \quad (42)$$

Thrust developed downstream of the point of separation is approximated empirically[100] by simulating the distribution depicted in Fig. 14;

$$(\Delta C_F)_s = [0.55(P_i + P_{0.95})(\epsilon_{0.95} - \epsilon_i) + 0.975P_a(\epsilon_e - \epsilon_{0.95})]/P_c \quad (43)$$

where

$$\epsilon_{0.95} - \epsilon_i = 0.417(\epsilon_i - 1) \text{ if } \epsilon_i < 0.377 + 0.623\epsilon_e$$

$$\epsilon_{0.95} - \epsilon_i = 0.69(\epsilon_e - \epsilon_i) \text{ if } \epsilon_i \geq 0.377 + 0.623\epsilon_e$$

As less data are available for contoured nozzles, no generalized expressions have been developed although limited studies have been conducted.[106,108]

Conclusion

Mathematical modeling techniques used to simulate the internal flowfields existing in solid-rocket combustion chambers are reasonably good for steady-state and transient flow conditions. Improvement could be accomplished by employing two-dimensional flow analyses. The uncertainties associated with the prediction of the response of burning front progress to such phenomena as mass flux, spin, un-

symmetrical thermal gradients, and high-pressure transients appear to require first consideration, although solutions to some or all of these uncertainties would be improved by two-dimensional analyses. Ballistic evaluation motor tests duplicating the augmentation environments further enhance full-scale motor performance predictions.

A considerable quantity of motor and nozzle efficiency data has been accumulated by the industry for contemporary designs. This information and experience has made it feasible to adjust theoretical specific impulse and thrust coefficient values and to predict rather accurately the performance of new but similar motor designs. Proven detailed analytical techniques are available for predicting deliverable specific impulse and nozzle performance. These account for the major contributing factors to the momentum losses encountered in solid rocket motors. Finally, the practice of scaling specific impulse demonstrated in a ballistic evaluation motor to that to be delivered by a full-scale propulsion system has proven satisfactory in performance predictions.

References

[1] Miller, W. H., "Design Criteria Monograph for Solid Rocket Motor Performance Analysis and Prediction," NASA Lewis Research Center, Cleveland, Ohio, to be published.

[2] Price, E. W., "Status of Solid Rocket Combustion Instability Research," NOTS TP 4275, Feb. 1967, U.S. Naval Ordnance Test Station, China Lake, Calif.

[3] Coates, R. R., and Horton, M. D., "Design Considerations for Combustion Stability," *Journal of Spacecraft and Rockets*, Vol. 6, No. 3, March 1969, pp. 296–302.

[4] Threewit, T. R., Rossini, R. A., and Uecker, R. L., "The Integrated Design Computer Program and the ACP-1103 Interior Ballistics Computer Program," STM-180, (AD 466965), Dec. 1964, Aerojet-General Corp.

[5] "Solid Propellant Rocket Motor Internal Ballistics Computer Program, (Program Manual)," RK-TR-67-7, (AD 822349), Sept. 1967, The Boeing Co., Seattle, Wash.

[6] "Grain Design and Internal Ballistics Evaluation Program, (IBM 7094 FORTRAN IV)," Program 64101, (AD 818321), July 1967, Hercules Inc., Bacchus Works, Magna, Utah.

[7] Hill, P. G. and Peterson, C. R., *Mechanics and Thermodynamics of Propulsion*, Addison-Wesley, Reading, Mass., 1965, pp. 353–424.

[8] Barrere, M. et al., *Rocket Propulsion*, D. Van Nostrand, New York, 1960, pp. 237–239.

[9] Bradley, H. H., Jr. and Price, E. W., "Flow of Gas in Tapered Channel with Mass Addition by George L. Dehority," Navweps Rept. 8606, NOTS TP 3626, Sept. 1964, U.S. Naval Ordnance Test Station, China Lake, Calif.

[10] Liepmann, H. W. and Roshko, A., *Elements of Gas Dynamics*, GALCIT Aeronautical Series, 3rd printing, Wiley, New York, Feb. 1960, pp. 39–61.

[11] Lewis, S. R., "Design of Solid Propellant Gas Generators for Transient Operation," ICRPG/AIAA 2nd Solid Propulsion Conference, Anaheim, Calif., June 6–8, 1967; Preprints available at Rocketdyne, Solid Rocket Division, McGregor, Texas.

[12] Barrett, D. H., "Design Criteria Monograph for Solid Rocket Igniters," NASA Lewis Research Center, Cleveland, Ohio, to be pulished.

[13] "Ballistic Evaluation of Propellants in Micro-Motors," No. S-49, (N65-13293), Oct. 1964, Rohm and Haas Co., Redstone Arsenal Research Div., Huntsville, Ala.

[14] Jessup, H. A. and VanWie, H. B., "Proposed Technique for Determination of End Pressure," CPIA 24, Sept. 1963, (AD 345567), CPIA Working Group on Static Testing.

[15] "Solid Propulsion Nomenclature Guide," CPIA 80, May 1965, (AD 465058), Chemical Propulsion Information Agency.

[16] Whitney, C. E. et al., "Scout Motor Performance Analysis and Prediction Study (PAPS)," CR-336, Dec. 1965, NASA.

[17] Brooks, W. T., private communication, Jan. 7, 1969, Rocketdyne, Solid Rocket Div., McGregor, Texas.

[18] Herty, C. H. and Ratliff, O. D., "Prediction of Ballistic Performance of Solid Propellant Rockets from Strand and Small-Scale Motor Tests," Publ. SPS-NDT/1A, (N-64740), *JANAF Symposia on Scale and Nondestructive Testing*, Sacramento, Calif., Johns Hopkins Univ., Md., Jan. 1960.

[19] Witcraft, G. M. and Liebman, M. E., "Correlation of Small Scale and Full Scale Rocket Motor Burning Rates," Publ. SPS-NDT/1A, (N-64740), *JANAF Symposia on Scale and Nondestructive Testing*, Sacramento, Calif., Johns Hopkins University, Md., Jan. 1960.

[20] Green, L., Jr., "Erosive Burning of Some Composite Solid Propellants," *Jet Propulsion*, Vol. 24, No. 1, Jan.-Feb. 1954, pp. 9–16.

[21] Heron, R., "Internal Ballistic Problems of Solid-Propellant Rocket Motors," *Rocket Propulsion Technology*, Vol. I, British Interplanetary Society, 1961.

[22] Marklund, T., "Propellant Erosion Studies," 1961, Research Institute of National Defense, Sweden.

[23] Marklund, T. and Lake, A., "Experimental Investigation of Propellant Erosion," *ARS Journal*, Vol. 30, No. 2, Feb. 1960.

[24] Dickinson, L. A., Jackson, E., and Odgers, A. L., "Erosive Burning of Polyurethane Propellants in Rocket Engines," *Eighth Symposium (International) on Combustion*, Williams and Wilkins Co., 1962, p. 754.

[25] Zucrow, M. J., Osborn, J. R., and Murphy, J. M., "An Experimental Investigation of the Erosive Burning Characteristics of a Nonhomogeneous Solid Propellant," *AIAA Journal*, Vol. 3, No. 3, March 1965, pp. 523–525.

[26] Kreidler, J. W., "Erosive Burning: New Experimental Techniques and Methods of Analysis," AIAA Paper 64-155, Palo Alto, Calif., 1964.

[27] Lenoir, J. M. and Robbillard, G., "A Mathematical Method to Predict the Effects of Erosive Burning in Solid-Propellant Rockets," *Sixth Symposium on Combustion*, Reinhold, New York, 1957, pp. 663–667.

[28] Peretz, A., "Experimental Investigation of the Erosive Burning of Solid-Propellant Grains with Variable Port Area," *AIAA Journal*, Vol. 6, No. 5, May 1968, pp. 910–912.

[29] Saderholm, C. A., "A Characterization of Erosive Burning for Composite H-Series Propellant," AIAA Solid-Propellant Rocket Conference, Palo Alto, Calif., Jan. 29–31, 1964.

[30] Viles, J. M., "Measurement of Erosive Burning Rates," TR-S-213, Jan. 1969, Rohm and Haas Co., Huntsville, Ala.

[31] Lawrence, W. J., Matthews, D. R., and Deverall, L. I., "The Experimental and Theoretical Comparison of the Erosive Burning Characteristics of Composite Propellants," AIAA Paper 68-531, Atlantic City, N.J., 1968.

[32] Von Elbe, G., "Theory of Solid Propellant Ignition and Response to Pressure Transients," CPIA 13, (AD 338667), July 1963, *Bulletin of the Interagency Solid Propulsion Meeting*, Seattle, Wash.

[33] Paul, B. E., Lovine, R. L., and Fong, L. Y., "A Ballistic Explanation of the Ignition Pressure Peak," AIAA Paper 64-121, Palo Alto, Calif., 1964.

[34] Parker, K. H., and Summerfield, M., "Response of the Burning Rate of a Solid Propellant to a Pressure Transient," AIAA Paper 66-683, Colorado Springs, Colo., 1966.

[35] Manda, L. J., "Compilation of Rocket Spin Data, Volume II: Literature Survey," Final Report, Contract NAS 1-6833 NASA CR 66641, (N68-34315), July 1968, Emerson Electric Co., St. Louis, Mo.

[36] Norton, D. J., Farquhar, B. W., and Hoffman, J. D., "Analytical Studies of the Interior Ballistics of Spinning Rocket Motors—A Literature Survey," TM 67-1, JPC 431, (AD 814933), Jan. 1967, Jet Propulsion Center, Purdue Univ., Lafayette, Ind.

[37] Northam, G. B. and Lucy, M. H., "On the Effects of Acceleration Upon Solid Rocket Performance," AIAA Paper 68-530, Atlantic City, N.J., 1968.

[38] Northam, G. B., "Effects of Steady-State Acceleration on Combustion Characteristics of an Aluminized Composite Solid Propellant," TN-D-4914, Dec. 1968, NASA.

[39] Whitesides, R. H., Jr. and Hodge, B. K., "Theoretical Study of the Ballistics and Heat Transfer in Spinning Solid Propellant Rocket Motors," Rept. U-68-20A, NASA-CR-66639, Aug. 1968, Huntsville Div., Thiokol Chemical Corp.

[40] Jones, H. G., "A Research Study to Advance the State-of-the-Art of Solid Propellant Grain Design," Summary Report E92-63, RTD-TDR-63-1049, (AD 420826), Oct. 1963, Elkton Div., Thiokol Chemical Corp., Elkton, Md.

[41] Saylak, D., "The Effects of Strain on the Burning Rate of Solid Propellants," CPIA 27, (AD 345530), Nov. 1963, *Bulletin of the Second ICRPG Working Group on Mechanical Behavior*, Hill Air Force Base, Utah.

[42] Pieper, J. L., "Performance Evaluation Methods for Liquid Propellant Rocket Thrust Chambers," CPIA 132, (X67-10715),

Nov. 1966, Interagency Chemical Rocket Propulsion Working Group on Performance Standardization.

[43] Pieper, J. L., "ICRPG Liquid Propellant Thrust Chamber Performance Evaluation Manual," CPIA 178, Sept. 1968, Performance Standardization Working Group, Interagency Chemical Rocket Propulsion Working Group on Performance Standardization.

[44] Hoglund, R. F., "Recent Advances in Gas-Particle Nozzle Flows," *ARS Journal*, Vol. 32, May 1962, pp. 662–671.

[45] Kliegel, J. R., "Gas Particle Nozzle Flows," *Ninth Symposium on Combustion*, Academic Press, New York, 1963, pp. 811–826.

[46] Crowe, C. T. et al., "Effect of Nozzle Pressure Level and Scale on Performance of Solid-Propellant Rocket Motors," Final Report UTC 2094-FR, (X65-16776), April 1965, United Technology Center, Sunnyvale, Calif.

[47] Hoffman, J. D., "An Analysis of the Effects of Gas-Particle Mixtures on the Performance of Rocket Nozzles," TM-63-1, (N63-17595), Jan. 1963, Jet Propulsion Center, Purdue Univ., Lafayette, Ind.

[48] "Recommended Procedure for the Measurement of Specific Impulse of Solid Propellants," CPIA 174, Aug. 1968, ICRPG Solid Propellant Rocket Static Test Working Group.

[49] Kliegel, J. R. et al., "One-Dimensional Two-Phase Reacting Gas Non-equilibrium Performance Program, Vol. I, Engineering and Programming Description," Rept. MSC-11780, Aug. 1967, TRW Systems, Redondo Beach, Calif.

[50] Kliegel, J. R. et al., "Axisymmetric Two-Phase Perfect Gas Performance Program, Vol. I, Engineering and Programming Description," Rept. MSC-11774, April 1967, TRW Systems, Redondo Beach, Calif.

[51] *JANAF Thermochemical Data Book*, (N-90810), Dow Chemical Co., Midland, Mich., Aug. 1963.

[52] Cherry, S. S., "Phase II Final Report—Screening of Reaction Rates," Rept. 08832-6002-T000, (AD 282795), Dec. 1967, TRW Systems.

[53] Zeleznik, F. J. and Gordon, S., "A General IBM 704 or 7090 Computer Program for Computation of Chemical Equilibrium Compositions, Rocket Performance, and Chapman-Jouguet Detonations," TN-D-1454, 1962, NASA.

[54] Zeleznik, F. J. and Gordon, S., "Supplement I," TN-D-1454, TN-D-1737, Oct. 1963, NASA; see Ref. 53.

[55] Hoffman, J. D. and Lorenc, S. A., "A Parametric Study of Gas-Particle Flows in Conical Nozzles," *AIAA Journal*, Vol. 3, No. 1, Jan. 1965, pp. 103–106.

[56] Bray, K. N. C. and Appleton, J. P., "Atomic Recombination in Nozzles, Methods of Analysis for Flows with Complicated Chemistry," Dept. of Aeronautics and Astronautics, Univ. of Southampton, England.

[57] Brown, B., "A Review of Multiphase Flow Through Converging-Diverging Rocket Nozzles," CPIA 44, (AD 359497), Proceedings of the First Meeting, CPIA Working Group on Thermochemistry, Silver Spring, Md., Feb. 1964.

[58] Moody, H. L. and Price, F. C., "The Prediction of Nozzle Material Performance for NASA's 260 SL-3 Motor," *Journal of Spacecraft and Rockets*, Vol. 6, No. 3, March 1969, pp. 273–279.

[59] Gale, W. H., "Development and Evaluation of the USAF Ballistic Test Evaluation System for Solid Rocket Propellants," SSD-TDR-62-45, (AD 276424), April 1962, Air Force Space System Div., Edwards, Calif.

[60] Peterson, J. A., "The Selection of the Optimum Solid Propellant," Fifty-Third National Meeting of the AIChE, American Institute of Chemical Engineers, New York, May 1964.

[61] Crowe, C. T. et. al., "Dynamics of Two-Phase Flow in Rocket Nozzles," Final Technical Report UTC 2102-FR, (AD 471996), Sept. 1965, United Technology Center, Div. of United Aircraft Corp., Sunnyvale, Calif.

[62] Geckler, R. D. and Sprenger, D. F., "The Correlation of Interior Ballistic Data for Solid Propellants," *Jet Propulsion*, Vol. 24, No. 1, Jan.-Feb. 1954, pp. 22–26.

[63] Gordon, L. J., "Ballistic Effect of Pyrolyzed Liner in Solid Propellant Motor Firings," *ARS Journal*, Vol. 30, No. 5, May 1960, pp. 502–503.

[64] "Thiokol 260-SL Subscale Nozzle Verification Program," Rept. Thio-6285-54869, NASA-CR-54869, (N68-17198), Jan. 1966, Thiokol Chemical Corporation, Brunswick, Ga.

[65] Wong, E. Y., "Solid Rocket Nozzle Design Summary," AIAA Paper 68-655, Cleveland, Ohio, 1968.

[66] Bartz, D. R., "A Simple Equation for Rapid Estimation of Rocket Nozzle Convection Heat Transfer Coefficients," *Jet Propulsion*, Vol. 27, No. 1, Jan. 1957, pp. 49–51.

[67] Hagewood, J. R., "Convergent-Divergent Nozzle Contour Optimization Techniques," BOE-D5-13300, (AD 812244L), Boeing Co., New Orleans, La.

[68] Farley, J. M. and Campbell, C. E., "Performance of Several Methods of Characteristics Exhaust Nozzles," TN D293, 1960, NASA.

[69] Rao, G. V. R., "Optimum Thrust Performance of Contoured Rocket Nozzles," (AD 319657), *LPIA—First Meeting JANAF Liquid Propellant Group, Vol. I*, Johns Hopkins Univ., Md., Nov. 1959.

[70] Malina, F. J., "Characteristics of the Rocket Motor Based on the Theory of Perfect Gases," *Journal of the Franklin Institute*, Vol. 230, 1940, pp. 433–454.

[71] Landsbaum, E. M., "Thrust of a Conical Nozzle," *ARS Journal*, Vol. 29, No. 3, March 1959, pp. 212–213.

[72] Rao, G. V. R., "Evaluation of Conical Nozzle Thrust Coefficient," *ARS Journal*, Vol. 29, No. 8, Aug. 1959, pp. 606–607.

[73] Lancaster, C. N. and Desjardins, S. P., "Investigation of the Effects of Various Nozzle Transition Arc Radius Ratios," Thio-1268-22182, March 1969, Wasatch Div., Thiokol Chemical Corp., Brigham City, Utah.

[74] Kordig, J. W. and Fuller, G. H., "Correlation of Nozzle Submergence Losses in Solid Rocket Motors," *AIAA Journal*, Vol. 5, No. 1, Jan. 1967, pp. 175–177.

[75] Kordig, J. W., private communication, Sept. 1969, Hercules Inc., Bacchus Works, Magna, Utah.

[76] Glauz, R. D., "Combined Subsonic-Supersonic Gas-Particle Flow," Preprint 1717-61, April 1961, American Rocket Society.

[77] Hoffman, J. D., "Analysis of the Flow of Gas-Particle Mixtures in Two-Dimensional and Axisymmetric Nozzles," TN BSD-TDR-62-144, (AD 294956), Dec. 1962, Aerojet-General Corp.

[78] Kleigel, J. R. and Nickerson, G. R., "Flow of Gas-Particle Mixtures in Axially Symmetric Nozzles," *Detonation and Two-Phase Flow*, edited by S. S. Penner and F. A. Williams, Academic Press, New York, 1962, pp. 173–194.

[79] Pai, S., *Introduction to the Theory of Compressible Flow*, D. Van Nostrand, Princeton, N.J., 1959, pp. 114–131.

[80] Oswatitsch, K. and Rothstein, W., "Flow Pattern in a Converging-Diverging Nozzle," TM 1215, March 1949, NACA.

[81] Sauer, R., "General Characteristics of the Flow Through Nozzles at Near Critical Speeds," TM 1147, June 1947, NACA.

[82] Hall, I. M., "Transonic Flow in Two-Dimensional and Axially-Symmetric Nozzles," *Quarterly Journal of Mechanics and Applied Mathematics*, Vol. XV, Pt. 4, 1962, pp. 487–508.

[83] Hopkins, D. F. and Hill, D. E., "Effect of Small Radius of Curvature on Transonic Flow in Axisymmetric Nozzles," *AIAA Journal*, Vol. 4, No. 8, Aug. 1966, pp. 1337–1343.

[84] Shapiro, A. H., *The Dynamics and Thermodynamics of Compressible Fluid Flows*, Vols. I and II, Ronald Press, New York, 1953, pp. 595–609.

[85] Ehlers, F. E., "The Method of Characteristics Applied to the Design of Supersonic Axially-Symmetric Nozzles," Document D2-2118, Aug. 1957, Boeing Airplane Co., Seattle, Wash.

[86] Beckman, C. C., private communication, June 1969, Rocket Propulsion Lab., Edwards Air Force Base, Calif.

[87] Crowe, C. T. and Willoughby, P. G., "A Study of Particle Growth in a Rocket Nozzle," *AIAA Journal*, Vol. 5, No. 7, July 1967, pp. 1300–1304.

[88] Carlson, D. J. and Hoglund, R. F., "Particle Drag and Heat Transfer in Rocket Nozzles," *AIAA Journal*, Vol. 2, No. 11, Nov. 1964, pp. 1980–1984.

[89] Cheung, H. and Cohen, N. S., "On the Performance of Solid Propellants Containing Metal Additives," AIAA Paper 64-116, Palo Alto, Calif., 1964.

[90] Sehgal, R., An Experimental Investigation of a Gas-Particle System, TR 32-238, (N62-11504), March 1962, Jet Propulsion Lab., California Institute of Technology, Pasadena, Calif.

[91] Crowe, C. T. et al., "Investigation of Particle Growth and Ballistic Effects on Solid-Propellant Rockets," UTC 2128-FR, (AD 486262), June 1966, United Technology Center, Sunnyvale, Calif.

[92] Cheung, H. and Cohen, N. S., "Performance of Solid Propellants Containing Metal Additives," *AIAA Journal*, Vol. 3, No. 2, Feb. 1965, pp. 250–257.

[93] Crowe, C. T. et al., "Measurement of Particle Drag Coefficients in Flow Regimes Encountered by Particles in a Rocket

Nozzle," UTC 2296-FR, March 1969, United Technology Center, Sunnyvale, Calif.

[94] Schlichting, H., *Boundary Layer Theory*, McGraw-Hill, New York, March 1958, pp. 97–98.

[95] McAdams, W., *Heat Transmission*, 3rd ed., McGraw-Hill, New York, 1954, pp. 265–266.

[96] Emmons, H. W., *Fundamentals of Gas Dynamics, High Speed Aerodynamics and Jet Propulsion*, Vol. 3, Princeton Univ. Press, Princeton, N.J., 1958, p. 725.

[97] Wiederkehr, R. R. V., "A General Method for Calculating the Specific Impulse of Propellant Systems," AR-1S-60, (N-84819), June 1960, Dow Chemical Co., Midland, Mich.

[98] Unger, E. W., "Heat Transfer to a Solid Propellant Rocket Motor Nozzle," Preprint 2333-62, (IAA Abstract 62-10244), Jan. 1962, American Rocket Society.

[99] Elliott, D. G., Bartz, D. R., and Silver, S., "Calculation of Turbulent Boundary Layer Growth and Heat Transfer in Axi-Symmetric Nozzles," TR 32-387, (N63-14465), Feb. 1963, Jet Propulsion Lab.

[100] Kalt, S. and Badal, D. L., "Conical Rocket Nozzle Performance Under Flow-Separated Conditions," *Journal of Spacecraft and Rockets*, Vol. 2, No. 3, May-June 1965, pp. 447–449.

[101] Garrett, J. W., Simmons, M., and Gobbell, W. C., "Exit Nozzle Flow Separation as Influenced by Nozzle Geometry, Fuel-Oxidizer Ratio, and Pressure Level," AEDC-TR-67-122, (AD 816650), July 1967, Arnold Engineering Development Center, Arnold Air Force Station, Tenn.

[102] Sutton, G. P., *Rocket Propulsion Elements*, Wiley, New York, April 1964, pp. 37–83.

[103] Arena, M. and Spiegler, E., "Separated Flow in Overexpanded Nozzles at Low Pressure Ratios," *The Bulletin of the Research Council of Israel, Sec. C, Technology*, 11C, April 1962, pp. 45–55.

[104] Altman, D. et al., *Liquid-Propellant Rockets*, Princeton Aeronautical Paperbacks, Princeton Univ. Press, Princeton, N.J., 1960.

[105] Bloomer, H. E., Antl, R. J., and Renas, P. E., "Experimental Study of Effects of Geometric Variables on Performance of Conical Rocket-Engine Exhaust Nozzles," TN-D-846, June 1961, NASA.

[106] Roschke, F. J. and Massier, P. F., "Flow Separation in a Contour Nozzle," *ARS Journal*, Oct. 1962, pp. 1612–1613.

[107] Campbell, C. E. and Farley, J. M., "Performance of Several Conical Convergent-Divergent Rocket-Type Exhaust Nozzles," TN-D467, Sept. 1960, NASA.

[108] Lawrence, R. A. and Weynand, E. E., "Factors Affecting Flow Separation in Contoured Supersonic Nozzles," *AIAA Journal*, Vol. 6, No. 6, June 1968, pp. 1159–1160.

MARCH 1970 J. SPACECRAFT VOL. 7, NO. 3

Astrionics Selection and Operation on Interplanetary Missions

ELLIS F. HITT* AND FRED G. REA†
Battelle Memorial Institute, Columbus, Ohio

Selection of astrionics subsystems for automated spacecraft designed for interplanetary missions is accomplished using evaluation techniques which consider mission requirements, mission event schedules, and spacecraft design characteristics. These techniques provide a measure of astrionics system performance, aid in evaluation of competitive subsystems and in the preliminary design of conceptual subsystems, and are used in determination of the effectiveness of specific navigation updating and midcourse correction schedules. Using computer programs implementing these techniques, various astrionic systems were evaluated on alternate mission schedules for a Jupiter flyby mission. Results illustrate the usefulness of the techniques for selection of astrionics configurations, and evaluation of mission operation schedules which consider subsystem operation times, navigation updating with Kalman filtered measurements from Earth-based radars and onboard electro-optical sensors, and midcourse correction schedules.

Nomenclature

D_T, D_V = degrees of freedom of the target miss and midcourse ΔV covariances, respectively
P_{FA} = probability of mission failure attributable to the astrionics system
P_{FR} = probability of failure attributable to lack of astrionics reliability
P_{FT} = probability of excessive target miss
P_{FV} = probability of failure due to having insufficient midcourse fuel
Prob (ψ,D) = probability a vector's magnitude will exceed ψ times the square root of the trace of its covariance matrix
W_{AC} = weight of attitude control subsystem
W_{AH} = weight of astrionics hardware (inertial sensing unit, computer, communications, and electro-optical components)
W_{AT} = $W_{AC} + W_{AH} + W_{DV} + W_{ES}$
W_{DV} = weight of midcourse correction subsystem
W_{ES} = weight of electrical energy source
ΔV = midcourse correction velocity vector
$\psi(P,D)$ = inverse function of Prob (ψ,D)

Presented as Paper 69-882 at the AIAA Guidance, Control, and Flight Mechanics Conference, Princeton, N.J., August 18–20, 1969; submitted August 25, 1969; revision received November 3, 1969. This paper is based on work accomplished by Battelle Memorial Institute under Contract NAS 12-550 for the NASA, Electronics Research Center, Cambridge, Mass.

* Senior Systems Engineer, Systems and Electronics Department, Columbus Laboratories.

† Senior Systems Engineer, Systems and Electronics Department, Columbus Laboratories. Member AIAA.

Introduction

THE complexity and cost of astrionics for automated spacecraft and launch vehicles requires careful evaluation prior to committing major expenditure of funds for new programs. Techniques developed for evaluation of strapdown guidance systems[1] are extended to permit evaluation of aided inertial guidance systems and subsequently the complete astrionics. It is assumed that the principal astrionics subsystems are located above the last powered launch vehicle stage. This approach includes the weight of the astrionics in the final injected payload weight. Therefore, the astrionics can be considered to provide all navigation, guidance, and control functions for the launch vehicle and spacecraft (as is done for the mission under consideration), or for the launch